

Quantum-Size Effects in the Visible Photoluminescence of Colloidal ZnO Quantum Dots: A Theoretical Analysis

R. Carmina Monreal,^{*,†} S. Peter Apell,[‡] and Tomasz J. Antosiewicz^{*,¶,‡}

[†]*Departamento de Física Teórica de la Materia Condensada C5 and Condensed Matter Physics Center (IFIMAC), Universidad Autónoma de Madrid, E-28049 Madrid, Spain*

[‡]*Department of Physics and Gothenburg Physics Centre, Chalmers University of Technology, SE-412 96 Göteborg, Sweden*

[¶]*Centre of New Technologies, University of Warsaw, Banacha 2c, 02-097 Warsaw, Poland*

E-mail: r.c.monreal@uam.es; tomasz.antosiewicz@uw.edu.pl

Abstract

ZnO has been known long since to be a highly efficient luminescent material. In the last years, the experimental investigation of the luminescent properties of colloidal ZnO nanocrystals in the nanometer range of sizes has attracted a lot of interest for their potential applications in light-emitting diodes and other optical devices and in this work we approach the problem from a theoretical perspective. Here, we develop a simple theory for the green photoluminescence of ZnO quantum dots (QDs) that allows us to understand and rationalize several experimental findings on fundamental grounds. We calculate the spectrum of light emitted in the radiative recombination of a conduction band electron with a deeply trapped hole and find that the experimental behavior of this emission band with particle size can be understood in terms of quantum size effects of the electronic states and their overlap with the deep hole. We focus the comparison of our results on detailed experiments performed for colloidal ZnO nanoparticles in ethanol and find that the experimental evolution of the luminescent signal with particle size at room temperature can be better reproduced by assuming the deep hole to be localized at the surface of the nanoparticles. However, the experimental behavior of the intensity and decay time of the signal with temperature can be rationalized in terms of holes predominantly trapped near the center of the nanoparticles at low temperatures being transferred to surface defects at room temperature. Furthermore, the calculated values of the radiative lifetimes are comparable to the experimental values of the decay time of the visible emission signal. We also study the visible emission band as a function of the number of electrons in the conduction band of the nanoparticle, finding a pronounced dependence of the radiative lifetime but a weak dependence of energetic position of the maximum intensity.

Keywords

Quantum dots, photoluminescence, zinc oxide

Introduction

ZnO has been known long since to be a highly efficient fluorescent material^{1,2} and as such proposed as an excellent candidate for light-emitting and optoelectronic devices.³ Many studies done in the past using single crystals and powders^{4,5} showed that when ZnO is excited with UV light across the bandgap, two emission bands appear. The narrow band, known as the exciton band, is at an energy close to the incident energy and originates from the radiative recombination of a photoexcited electron with a valence band hole. The broad band is in the visible and is called the green luminescence band because of its color. It is associated with the existence of intrinsic lattice defects, vacancies or impurities^{2,4,6,7} that can trap charge carriers and for this reason it is also called the defect luminescence band.

In the last years the luminescent properties of colloidal ZnO quantum dots (QDs) in the nanometer range of sizes have been investigated. The two bands also appear in this case and their relative intensity is extremely dependent on whether the nanoparticles are in an atmosphere with or without the presence of oxygen.⁸⁻¹⁷ Under aerobic conditions the visible band is prominent while the exciton band is a weak feature. However, under anaerobic conditions and upon irradiation with UV light, the visible emission band quenches as the exciton band increases in intensity.⁸⁻¹⁵ Furthermore, an infrared absorption band develops due to the accumulation of electrons in the conduction band that leads to the formation of a local surface plasmon resonance in the nanoparticle.¹⁶⁻¹⁸ Admission of oxygen provokes the opposite effect: the luminescent exciton emission disappears as the visible emission band recovers in intensity^{12,13} and the infrared absorption is also quenched.¹⁷

There are few experiments analyzing in detail the size dependence of the luminescent properties of ZnO QDs.⁸⁻¹¹ Such dependence is interesting since for these nanocrystals the size-quantization of the energy levels of electrons and holes is expected to determine their emission properties. The most extensive experiments were conducted in air for suspensions of ZnO nanoparticles in 2-propanol or ethanol in,^{10,11} where the intensity and the position of the visible band, as well as the decay time of the luminescent signal were monitored as a

function of size at room temperature. It was found that, as the nanoparticle size increases, the intensity of the band decreases, its position red shifts and the decay time increases, in accordance with previous observations.^{8,9} Also, the intensity and the decay time are very dependent on temperature: the intensity decreases by a factor of 5 and the decay time increases by approximately the same factor as the temperature increases from 4 K to room temperature.¹⁰ Up to our knowledge, the evolution of the visible luminescence signal with nanoparticle size has not yet been studied under anaerobic conditions with the same detail, probably because of its low intensity. Even for a given size, there are contradictory experiments concerning the shift of this band as the crystal becomes charged: while a blue shift is reported in,^{12,14,17} other Authors observed essentially no shift.¹³

The current theoretical investigation of colloidal QDs is focused on calculations of the electronic band structure of clusters with sizes smaller than 3 nm in diameter, with and without ligands at the surface, and at different levels of sophistication (we refer the reader to references^{19,20} and references therein) but such calculations cannot be extended to larger systems nowadays. In this work we attack the problem from a different perspective and develop a simple theory for the defect photoluminescence of QDs that allows us to understand and rationalize several experimental findings on fundamental grounds. Using Fermi's golden rule together with a simple model for the quantized electronic states, we analyze theoretically the characteristics of the visible emission band of ZnO QDs and their evolution with particle size. We focus on comparing our results with the detailed experiments of van Dijken et al.^{10,11} performed for ZnO nanoparticles in ethanol under aerobic conditions. The behavior of the spectral characteristics with particle size can be understood in terms of quantum size effects and the experiments at room temperature are reproduced more accurately by assuming the hole to be localized at the surface of the nanoparticle. Furthermore, the theoretical values of the radiative lifetime are comparable to the experimental values of the decay time. Based on our results, we suggest that the anomalous dependence of the decay time with temperature found by van Dijken et al.¹⁰ can be the effect of an increasing probability for the holes to be

trapped at the surface with increasing temperature. We also study the visible emission band as a function of the number of electrons in the nanoparticle finding a pronounced dependence of the radiative lifetime. We conclude that a better experimental characterization of the distribution of traps and the charge of the nanoparticles is essential to fully understand and control their emission properties.

Theory

Although there has been some controversy concerning the origin of the mechanism of the visible luminescence of ZnO, whether it is due to the radiative recombination of (i) a delocalized electron with a deeply trapped hole or (ii) a deeply trapped electron with a delocalized hole,^{10,13,21} it is now well established that mechanism (i) is dominant^{11,15,17} and in this work we adhere to this picture.

Our system consists of ZnO spheres of radius R in a medium characterized by its dielectric permittivity ϵ_m . When the sphere is illuminated with light of energy $\hbar\omega_{in}$ across the bandgap, a photon is absorbed exciting an electron to the conduction band and leaving a hole in the valence band. Some of the holes can be transferred very quickly to hole traps while some of the electrons can be scavenged by oxygen adsorbed at the nanoparticle surface, especially for particles in air, before light emission takes place. Therefore the number of electrons N_e and the number of holes N_h participating in the subsequent luminescent process are in general different. Since the charge and the number and distribution of hole traps are not well characterized experimentally, we need some simple but reasonable assumptions for N_e and N_h . Given that the exciton emission band is very weak when the nanoparticles are in air, we assume that all the created holes are transferred to hole traps. Then N_h equals the number of absorbed photons (per photon incident onto the sphere): $N_h = \frac{\sigma_{abs}(\omega_{in}, R)}{2\pi R^2}$, where $\sigma_{abs}(\omega_{in}, R)$ is the absorption cross section of a ZnO sphere of radius R . With respect to the number of electrons in the conduction band we assume either of two cases in which (a) N_e

is independent of size or (b) the electronic density $n_e = 3N_e/(4\pi R^3)$ is independent of size. In all cases we consider the electronic system to be in its ground state in the conduction band when light emission occurs. We work at $T = 0$ K but our results are also valid at room temperature since the excitation energies of the QDs are typically of $\simeq 0.1$ eV and therefore larger than the thermal energy at room temperature.

To study steady-state luminescence, we calculate the probability per unit time that a conduction band electron fills a deep hole with emission of a photon of frequency ω using Fermi's golden rule

$$\frac{1}{\tau_{ph}} = \frac{2\pi}{\hbar} \sum_{photons} \sum_i f(e_i) |M_{h,i}|^2 \delta(e_h - e_i + \hbar\omega), \quad (1)$$

where $\sum_{photons}$ indicates summation over all possible photon states, \sum_i indicates summation over all possible states i of a conduction electron, $f(e_i)$ is the Fermi factor giving the occupancy of state i of energy e_i , the final state h is the trapped-hole state of energy e_h and the δ -function expresses energy conservation. The matrix elements $M_{h,i}$ for the transition are

$$M_{h,i} = \frac{e}{2m_e^*c} \langle \Psi_h | \hat{p} \cdot \vec{A}_\mu^* + \vec{A}_\mu^* \cdot \hat{p} | \Psi_i \rangle. \quad (2)$$

In eq. (2) e and m_e^* are the charge and effective mass, respectively, of a conduction band electron, c is the speed of light, $|\Psi_i\rangle$ and $|\Psi_h\rangle$ are the electronic initial and the hole final states, respectively, $\hat{p} = -i\hbar\vec{\nabla}$ is the momentum operator and \vec{A}_μ is the vector potential of the electromagnetic field with polarization μ . In the Coulomb gauge $\vec{A}_\mu^* = i\frac{c}{\omega}\vec{E}_\mu^*$, \vec{E}_μ being the electric field vector, so that $M_{i,h}$ is rewritten as

$$M_{h,i} = \frac{e\hbar}{2m_e^*\omega} \langle \Psi_h | \vec{\nabla} \cdot \vec{E}_\mu^* + 2\vec{E}_\mu^* \cdot \vec{\nabla} | \Psi_i \rangle. \quad (3)$$

The electric field \vec{E}_μ is defined except for a normalization constant, $\vec{E}_{0\mu}$, which is obtained with the condition of having one photon of energy $\hbar\omega$ in the quantization volume V , so that

$|\vec{E}_{0\mu}|^2/(8\pi) = \hbar\omega/V$. Next, we perform the sum over photon states as

$$\frac{1}{V} \sum_{photons} \rightarrow 2 \int \frac{d^3\vec{k}_{ph}}{(2\pi)^3} = 2 \times \frac{4\pi}{(2\pi c)^3} \int d\omega \omega^2, \quad (4)$$

where the factor of 2 comes from polarization, \vec{k}_{ph} is the photon wave vector and the last identity is appropriate for the problem of full spherical symmetry (no preferential direction in space) in vacuum that we address in this work. Substituting eqs. (3-4) into eq. (1) and collecting all the prefactors we obtain

$$\frac{1}{\tau_{ph}} = \frac{4e^2}{m_e^{*2}c^3} \int_0^\infty d(\hbar\omega) \hbar\omega \sum_i f(e_i) |\tilde{M}_{h,i}|^2 \delta(e_h - e_i + \hbar\omega), \quad (5)$$

with the matrix elements given simply by

$$\tilde{M}_{h,i} = \langle \Psi_h | \vec{\nabla} \cdot \vec{E}^* + 2\vec{E}^* \cdot \vec{\nabla} | \Psi_i \rangle, \quad (6)$$

where in a time-reverse picture, the electric field \vec{E} is the total one inside the sphere corresponding to an outgoing electromagnetic plane wave of unit amplitude.

From eq. (5) we obtain the visible luminescence spectrum as the number of emitted photons with energies between $\hbar\omega$ and $\hbar(\omega + d\omega)$ per unit time and per photon incident onto the sphere as

$$\frac{dI_{VL}}{d(\hbar\omega)} = \frac{\sigma_{abs}(\omega_{in}, R)}{2\pi R^2} \times \frac{4e^2}{m_e^{*2}c^3} \hbar\omega \sum_i f(e_i) |\tilde{M}_{h,i}|^2 \delta(e_h - e_i + \hbar\omega), \quad (7)$$

the first factor on the right hand side of eq. (7) being the number of holes per photon incident onto the nanosphere. Note here that the assumption that all holes are deeply trapped only affects the intensity of the signal but not its spectrum nor the value of the radiative decay time, both given by eq. (5). We next give details of how we calculate each of the terms in eqs. (6) and (7).

The normalized electric field inside the nanoparticle induced by an x-polarized plane wave, can be written in the dipole approximation, due to the small sizes of interest here, as

$$\vec{E}(r, \theta, \varphi) = \left(1 - \frac{\alpha(\omega, R)}{R^3}\right) (\sin \theta \cos \varphi \hat{i}_r + \cos \theta \cos \varphi \hat{i}_\theta - \sin \varphi \hat{i}_\varphi), \quad (8)$$

in spherical coordinates, with \hat{i}_r , \hat{i}_θ and \hat{i}_φ being the unitary vectors. The polarizability of the sphere $\alpha(\omega, R)$ enters into the evaluation of \vec{E} . We assume it is set by these electrons in the conduction band that can participate in the emission event (i.e. those not scavenged by oxygen) and, accordingly, it is given by²²⁻²⁴

$$\alpha(\omega, R)/R^3 = \frac{\epsilon(\omega) - \epsilon_m + 2\frac{d_\theta(\omega, R)}{R}}{\epsilon(\omega) + 2\epsilon_m + 2\frac{d_\theta(\omega, R)}{R}}, \quad (9)$$

where $\epsilon(\omega)$ is the local permittivity of ZnO,

$$\epsilon(\omega) = \epsilon_\infty - \frac{\omega_p^2}{\omega^2 - \left(\frac{\Delta}{\hbar}\right)^2 + i\omega\gamma_b}, \quad (10)$$

ϵ_m is the permittivity of the medium surrounding the sphere (assumed to be frequency independent), ϵ_∞ is the high-frequency permittivity of ZnO, ω_p is the plasma frequency with $\omega_p^2 = \frac{4\pi n_e e^2}{m_e^*}$. Δ is the average distance between the conduction band levels defined as²⁵

$$\Delta = \hbar\omega_p \frac{R_0}{R}, \quad (11)$$

where R_0 can be estimated from a simple model²⁶ as $R_0 = \sqrt{\frac{3\pi a_0}{4m_e^* k_F}}$, with m_e^* being the effective electron mass (in units of the electron mass), a_0 being the Bohr radius and $k_F = (3\pi^2 n_e)^{\frac{1}{3}}$. The the complex length $d_\theta(\omega, R)$ takes into account the effects of diffuse surface scattering of the electrons,^{23,24} which is significant in low charge carrier density systems such as ZnO here considered.

The electronic states appearing in eq. (6) should be orthonormal because they should

be eigenfunctions of the same Hamiltonian. We take care of this very important fact in an approximate way. We start by considering the conduction band electrons as free-electrons confined by an infinite potential well at the surface of the nanosphere. These states are orthonormal and described by $|\phi_{lnm}\rangle$ for quantum numbers (lnm) , where (lm) are the angular momentum quantum numbers and n quantizes the energy for each l (energies e_{ln}). The corresponding wave functions, expressed in spherical coordinates, are

$$\phi_{lnm}(r, \theta, \varphi) = N_{ln} j_l \left(\rho_{ln} \frac{r}{R} \right) Y_l^m(\theta, \varphi), \quad (12)$$

where N_{ln} is the normalization constant, ρ_{ln} is the n -order zero of the spherical Bessel function $j_l(\rho)$ and $Y_l^m(\theta, \varphi)$ is the spherical harmonic. The corresponding eigenenergies (measured with respect to the bottom of the conduction band) are

$$e_{ln} = \frac{\hbar^2 \rho_{ln}^2}{2m_e^* R^2}. \quad (13)$$

The nature of the trap is still under debate and several proposals can be found in the literature such as Cu impurities,⁶ Zn vacancies²⁷ or oxygen vacancies¹⁰ among others. In the case of colloidal QDs, the chemical nature of surface ligands is known to play a role in their luminescent properties.²⁸ Therefore, in order to keep the problem as simple as possible, and since the energy of the deep hole is approximately in the middle of the band gap, we describe the deep hole state by the hydrogenic wave function

$$\phi_h(\vec{r}) = \frac{\alpha_h^{3/2}}{\sqrt{\pi}} e^{-\alpha_h |\vec{r} - \vec{a}|}, \quad (14)$$

with $\alpha_h = \sqrt{2m_h e_b / \hbar^2}$, m_h being the hole mass and e_b being its binding energy. When e_h is referred to the bottom of the conduction band, like e_{ln} , $e_b = E_g + e_h$, E_g being the band gap of ZnO. The deep hole is localized at a point \vec{a} inside the sphere that we will take as a parameter. Obviously, this hole state is not, in general, orthogonal to the conduction

band states of eq. (12). Next, we proceed to construct an orthonormal set of orbitals $\{\Psi_\alpha\}$ from the non-orthogonal set $\{\phi_\beta\}_{\{\beta=h,(lnm)\}}$ by means of the symmetrical orthogonalization procedure proposed by Löwdin:²⁹

$$\Psi_\alpha = \sum_{\beta} (\mathbf{S}^{-1/2})_{\alpha,\beta} \phi_\beta, \quad (15)$$

where \mathbf{S} is the overlap matrix with matrix elements $S_{\alpha,\beta} = \langle \phi_\alpha | \phi_\beta \rangle$. As a further approximation we assume all the off-diagonal matrix elements of \mathbf{S} to be small and expand $\mathbf{S}^{-1/2}$ in powers of the overlap integrals. Up to order $\mathcal{O}S_{\alpha,\beta}^2$ we get

$$(\mathbf{S}^{-1/2})_{\alpha,\beta} \approx \delta_{\alpha,\beta} - \frac{1}{2} \mathbf{S}_{\alpha,\beta}, \quad (16)$$

this approximation being especially useful for $a \neq 0$ because it makes possible to obtain an analytical expression for eqs. (5) and (6). Using it, the matrix elements $\tilde{M}_{h,i}$ of eq. (6) between orthogonal orbitals can be easily expressed in terms of the corresponding ones for non-orthogonal orbitals as

$$\tilde{M}_{h,(lnm)} = M_{h,(lnm)}^{n-o} - \frac{1}{2} \sum_{l'n'm'} S_{h,(l'n'm')} M_{(l'n'm'),(lnm)}^{n-o}, \quad (17)$$

with the superscript $n-o$ indicating that eq. (6) is to be evaluated between the non-orthogonal states of eqs. (12) and (14). The details of this calculation are given in the Supplemental Information.

The derivation above strictly holds for ideally spherical nanoparticles. For real spheres, however, because of the unavoidable existence of imperfections in their shape and morphology, it is nearly impossible to calculate a detailed level distribution. A common approach has been to assume the level distribution to be completely random.^{26,30} On the other hand, the hole state has a large width. It is known that electron-hole recombination at a defect site results in large reorganization of the local charge and, consequently, strong vibronic

transitions. We take care of these effects by making use of the identity

$$\delta(e_h - e_{ln} + \hbar\omega) = \int de \delta(e - e_{ln}) \int de' \delta(e' - e_h) \delta(e' - e + \hbar\omega), \quad (18)$$

and then substituting the function $\delta(e - e_{ln})$ by a gaussian distribution of probability function as³⁰

$$\delta(e - e_{ln}) \rightarrow G(e - e_{ln}) = \frac{1}{\sigma\sqrt{2\pi}} \exp\left[-\frac{(e - e_{ln})^2}{2\sigma^2}\right], \quad (19)$$

for the conduction band states and likewise for the deep hole state

$$\delta(e' - e_h) \rightarrow G(e' - e_h) = \frac{1}{\sigma_h\sqrt{2\pi}} \exp\left[-\frac{(e' - e_h)^2}{2\sigma_h^2}\right]. \quad (20)$$

An appropriate value for σ is $\sigma = \Delta/2$,³⁰ Δ being the average distance between the conduction band levels near their Fermi energy defined by eq. (11). We take $\sigma_h \approx 0.1 - 0.2$ eV, a typical value for vibrational energies. However, we assume for simplicity that the matrix elements can be calculated by means of eq. (17), which implies that matrix elements are not very sensitive to changes in nanoparticle radii by $\approx 7\%$ ³⁰ or to changes in the wave function of the deeply trapped hole.

Results and discussion

We perform calculations for the case of ZnO nanospheres in ethanol using the values: $E_g = 3.44$ eV, $m_e^* = 0.28m_e$, $\gamma_b = 0.1$ eV, $\epsilon_\infty = 3.72$ and $\epsilon_m = 1.85$. The parameters for the deep hole are $m_h = m_e$ and $\epsilon_h = -1.95$ eV (measured with respect to the bottom of the conduction band) taken from experiments.¹¹ In all the calculations to be presented in this work, we include in eq. (17) states ($l'n'm'$) with $n' \leq 7$ for each of the quantum numbers ($l'm'$) and this is enough for obtaining converged results. In the following, states (ln) will be denoted according to the standard notation as nS for $l = 0$, nP for $l = 1$, nD for $l = 2$ etc.

To check the accuracy of eq. (16) we present in Figure 1a,b the overlap integrals $S_{h,(lnm)}$

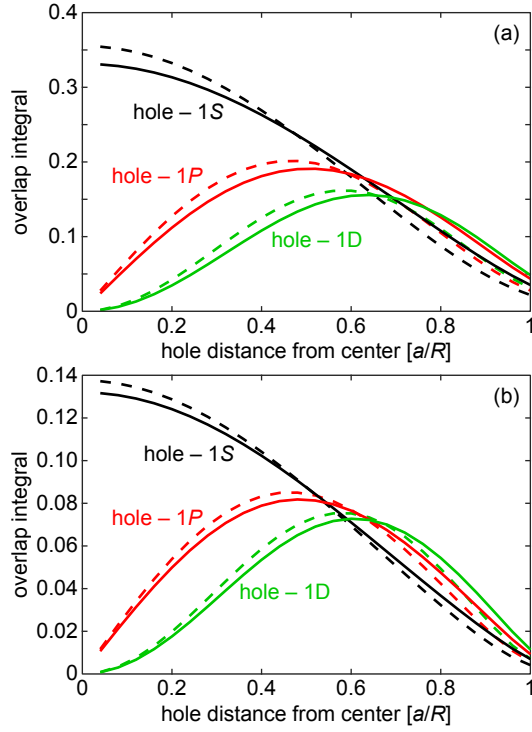


Figure 1: The overlap integrals between the deep hole at position a/R from the QD center and the $1S$ (black lines), $1P$ (red lines) and $1D$ (green lines) states of the conduction band electrons as a function of the distance of the hole to the surface of the sphere. Continuous lines: step potential barrier of height $V_0 = 4$ eV, dashed lines: infinite barrier at the surface of the nanoparticles. (a) $R = 2$ nm; (b) $R = 4$ nm.

for $l = 0, 1, 2$, $n = 1$ and $m = 0$, as a function of the distance a of the deep hole to the sphere center, for $R = 2$ nm and $R = 4$ nm respectively. We note that the overlap of the deep hole with the nS states of the conduction band electrons is ≈ 0.4 near the center and then decreases as a approaches the sphere surface. Therefore, while the approximation of eq. (16) is a good one near the surface, it might not be so good near the sphere center, especially for the smallest size. For $a = 0$ it is not difficult to obtain corrections to eq. (16) up to the order $\mathcal{O}S_{\alpha,\beta}^4$ and we have checked that this does not change the order of magnitude of the results. Nevertheless, we restrict our calculations to $a \geq 0.2R$. Figure 1 also shows a comparison of the overlap integrals assuming that the conduction electrons are confined by an infinite barrier (dashed lines) or by a step potential barrier of height $V_0 = 4$ eV (continuous lines).^{30,31} The small changes we see motivate our use of infinite barrier model, that is much simpler for analytical and computational purposes.

We first present results under the assumption (a) that the number of electrons in the conduction band is a small number independent of particle size. To demonstrate the importance of orthogonalization effects, Figure 2a,b shows calculations of the visible luminescence spectra, using orthogonal (continuous lines) and non-orthogonal (dashed lines) states, for $N_e = 4$ (2 electrons in the $1S$ state and 2 electrons in the $1P$ state), $R = 2, 3$ and 4 nm, $\sigma_h = 0$ and for $a = 0.2R$ in Figure 2a and $a = 0.8R$ in Figure 2b. Note that the non-orthogonal calculation overestimates the spectra by roughly a factor of 4 and, consequently, the radiative lifetimes would be underestimated by the same factor. The peaks in Figure 2a originate from the radiative recombination of the electron in the $1P$ state with the trapped hole of the same spin. The peak intensity decreases and its position shifts to lower energy with increasing size, as in the experiments. The shift to lower energy with increasing size is predicted by eq. (13) for the eigenenergies. The decrease in intensity is the consequence of the decrease in the overlap between electron and hole states with increasing size, compare Figure 1a and b, and the matrix elements appearing in eq. (17) behave in the same way. Hence this simple model reproduces the experimental behavior of the evolution of position and intensity of

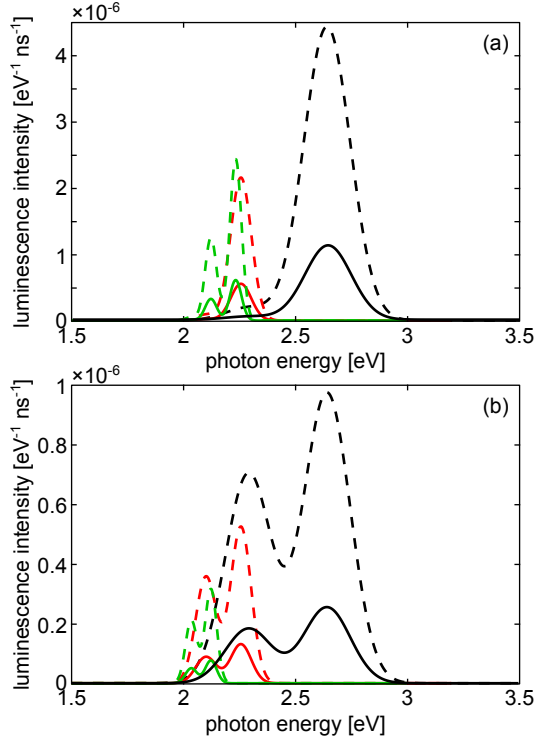


Figure 2: Visible luminescence spectra of nanospheres of $R = 2$ nm (black lines), $R = 3$ nm (red lines) and $R = 4$ nm (green lines), all having $N_e = 4$ electrons in the conduction band, calculated using orthogonal (continuous lines) and non-orthogonal (dashed lines) orbitals and $\sigma_h = 0$. The hole is localized in (a) at $a = 0.2R$ and in (b) at $a = 0.8R$. A proper orthogonalization of the involved states decreases the emission probabilities and, consequently, increases the radiative lifetimes, by a factor of 4. Only $1P$ states can contribute to radiative decay of the hole in (a) while $1S$ states can also do it in (b). Therefore the shape of the emission band depends on the hole position.

the steady-state green luminescence with particle size at room temperature.⁸⁻¹¹ The small shoulder to the left of the peak in Figure 2a originates from the radiative recombination of the electron in the $1S$ state with the trapped hole of the same spin. This process, that is strictly forbidden if the hole is localized at $a = 0$, shows as a faint feature for small values of a but gets important if the deep hole is localized near the nanoparticle surface, as can be appreciated in Figure 2b, where both peaks are of nearly the same intensity. Nevertheless the relative intensity of both peaks does not change much for $a \geq 0.5R$

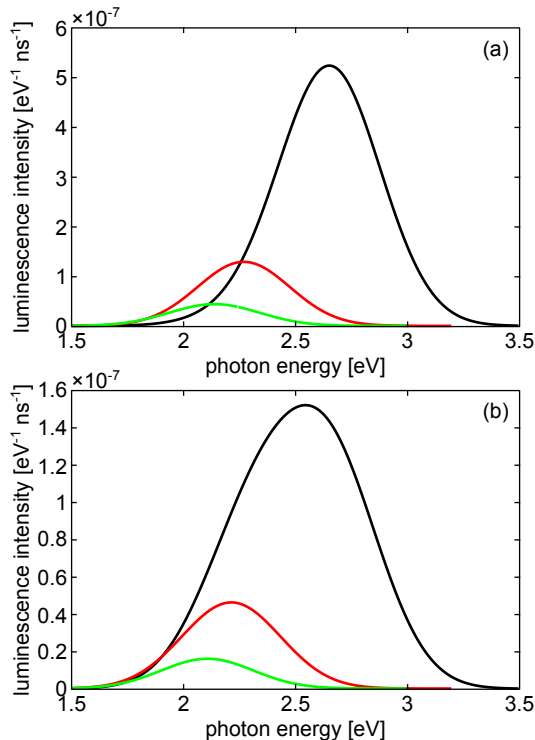


Figure 3: Visible luminescence spectra of nanospheres of $R = 2$ nm (black lines), $R = 3$ nm (red lines) and $R = 4$ nm (green lines), all having $N_e = 4$ electrons in the conduction band, assuming the hole to be localized in (a) at $a = 0.2R$ and in (b) and $a = 0.8R$ with an energy broadening of the hole $\sigma_h = 0.2$ eV. The emission bands of Figure 2 evolve into broad continuous bands, with both the maximum intensity and its energetic position decreasing with increasing size, in qualitative agreement with experiments.

The calculations of Figure 2 are for a hole state having zero width. Figure 3 displays the photoluminescence spectra of eq. (7) for the same parameters as in Figure 2 but including an energy broadening of the deep hole of $\sigma_h = 0.2$ eV, where it can be observed how the atomic-like peaks merge and form a continuous broad band. Although the behavior with particle size

of this band follows the experimental trends mentioned above, a more quantitative analysis shows that the relative changes are too quick in comparison with experiments. The same happens if we assume to have $N_e = 2$ in the QDs (not shown here). Figure 3 of ref.¹⁰ shows a quick decrease of the peak intensity with increasing size for radii smaller than ca. 1.5 nm which can be modeled by the present approximation, but this quick decrease is followed by almost constant values of the intensity for radii increasing up to 3.5 nm, while a continuous decrease is obtained in the calculations. The quick decrease in peak energy with increasing radius is also not seen in the experiments,¹⁰ where this energy decreases from ca. 2.4 eV for the smallest size to ca. 2.2 eV for the larger radius.

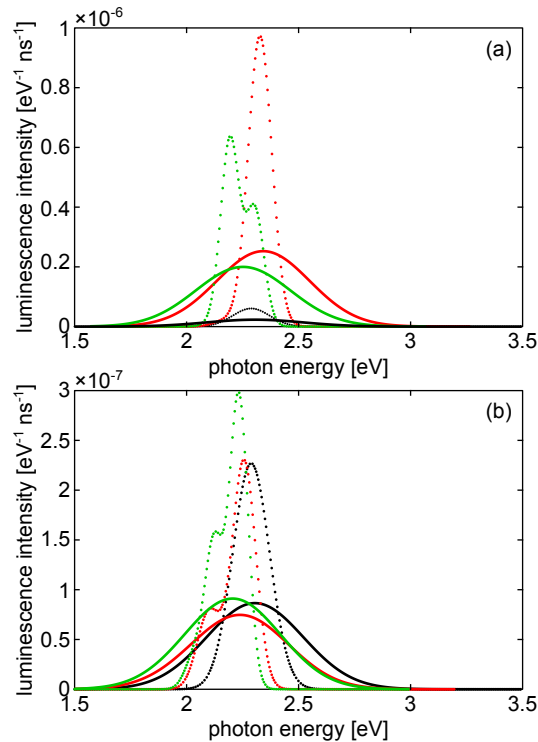


Figure 4: Visible luminescence spectra of nanoparticles of $R = 2$ nm (black lines), $R = 3$ nm (red lines) and $R = 4$ nm (green lines), all having the same density $n_e = 0.6 \times 10^{20} \text{ cm}^{-3}$ of electrons in the conduction band, assuming the hole to be localized in (a) at $a = 0.2R$ and in (b) at $a = 0.8R$, for $\sigma_h = 0$ (dotted lines) and $\sigma_h = 0.2$ eV (continuous lines). The evolution of the intensity of the emission bands with QD size is very different depending on where inside the nanoparticle is the hole localized. A better agreement with the experiments at room temperature¹⁰ is obtained assuming the hole is located near the surface, as in (b).

We then turn to our assumption (b) and consider that the density of conduction band elec-

trons n_e is independent of particle size. This is motivated by the fact that well characterized ZnO colloidal QDs in toluene, with sizes ranging from 2 to 6 nm in radii, can be charged, under anaerobic conditions, all to the same maximum electron density of $n_e = (1.4 \pm 0.4) \times 10^{20} \text{ cm}^{-3}$ ¹⁸ and in previous works we used the lower limit of this density to reproduce the IR absorption properties of these QDs.^{23,24,30} Guided by these maximum values, we consider the aerated QDs to have approximately one half of that density. Actually, since in our calculations we always have an even number of conduction electrons (half of each spin) and the minimum value of N_e is 2, the minimum density we consider is $n_e = 0.6 \times 10^{20} \text{ cm}^{-3}$ corresponding to 2 electrons in a sphere of $R = 2$ nm. Under the assumption that all QDs have this same density of electrons in the conduction band, a sphere of $R = 3$ nm has $N_e = 6$ electrons and a sphere of $R = 4$ nm has $N_e = 16$ electrons.

The visible photoluminescence spectra for equal electron density are presented in Figure 4a,b, for $a = 0.2R$ and $a = 0.8R$ respectively. Looking at the results for $\sigma_h = 0$ (dots), we only see one small peak at $\omega \simeq 2.3$ eV for $R = 2$ nm which originates from the electron in the $1S$ level. As we said above, this transition would be strictly forbidden if the hole was localized at the sphere center. Consequently, this feature is small for $a = 0.2R$ but not for $a = 0.8R$. For $R = 3$ nm, the prominent peak at $\omega \simeq 2.25$ eV in Figure 4 originates from the radiative decay of electrons in the $1P$ level while the shoulder at $\omega \simeq 2.1$ eV originates from electrons in the $1S$ level. For $R = 4$ nm the conduction band levels $1S$, $1P$ and $1D$ are populated with electrons and the corresponding features are seen in the photoluminescence spectra. Therefore, as size increases, the energy levels move down in energy but simultaneously higher energy levels become populated with electrons with the net effect being a slow variation of the position of the maximum with size. In fact, when we give a line broadening to the hole, the atomic-like features merge into broad bands with maxima at energy positions that decrease with increasing radius as before but at a pace more in accordance with experiments. The values of these maxima in Figure 4b are $\omega_{max} \simeq 2.31$ eV, $\omega_{max} \simeq 2.24$ eV, and $\omega_{max} \simeq 2.21$ eV, for $R = 2, 3$ and 4 nm, respectively. With respect to the dependence

of the maximum intensity on size, we note in Figure 4a that the peak of the $R = 2$ nm nanosphere is too small for $a = 0.2R$, and the experimental characteristics of a weak dependence of intensity on size in the range of sizes $1.5 \text{ nm} \leq R \leq 3.5 \text{ nm}$ is best reproduced if we assume the deeply trapped hole to be localized near the surface. This weak dependence is the net effect of the competition between decreasing overlap and increasing population of high energy levels with increasing size. Therefore, these calculations confirm the conclusions of van Dijken et al.¹⁰ showing evidence of fast surface trapping of holes in the trap emission process. It is also experimentally known that passivation of surface defects quenches the visible photoluminescence.^{17,28} The values of the radiative lifetimes for the cases in Figure 4b are $\tau_{ph} = 0.53 \text{ } \mu\text{s}$, $0.89 \text{ } \mu\text{s}$ and $0.98 \text{ } \mu\text{s}$ for $R = 2, 3$ and 4 nm respectively, increasing with increasing size as in the experiment, see Figure 4 of ref.¹⁰ Moreover, a value of $\tau = 1.34 \text{ } \mu\text{s}$ was measured for $R = 3$ nm and $\tau = 0.92 \text{ } \mu\text{s}$ for $R = 1$ nm at room temperature, both comparable to our calculation.

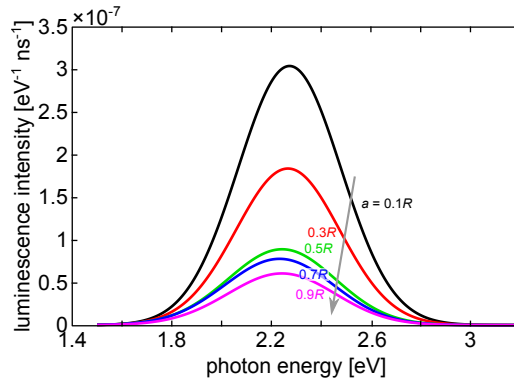


Figure 5: Visible luminescence spectra of nanoparticles of $R = 3$ nm with an electron density of $n_e = 0.6 \times 10^{20} \text{ cm}^{-3}$, $\sigma_h = 0.2 \text{ eV}$, for an increasing hole – QD-center distance a . The intensity decreases and the radiative lifetime increases (both with increasing a) by approximately the same factor as the corresponding experimental magnitudes do when the temperature is increased from 4 K to room temperature. This suggests that the holes are predominantly trapped at the particle center at low temperatures but at the particle surface at room temperature.

Based on the results presented above, we now give a possible reason for the experimentally observed behavior of the visible luminescence spectra and radiative lifetimes of the aerated QD with temperature presented in Figures 5B and 6 of van Dijken et al.¹⁰ for nanoparticles

of $R = 3$ nm. Figure 5 displays calculated spectra for nanospheres of $R = 3$ nm for different values of the position of the hole within the particle. It is interesting to note the fast decrease of the maximum intensity as the hole moves from the center to the surface, the factor of 5 difference we find here being reminiscent of the same fast decrease of the experimental intensity with increasing temperature shown in Figure 5B of van Dijken et al.¹⁰ Furthermore, the decay of the visible emission signal is found to be single exponential at very low and at room temperatures with values of the decay time of $0.275 \mu\text{s}$ and $1.34 \mu\text{s}$ at $T = 4$ K and room temperature, respectively. The theoretical values of the radiative lifetime are $0.24 \mu\text{s}$ and $1.14 \mu\text{s}$ for $a = 0.1R$ and $a = 0.9R$, respectively, and are comparable to the experimental values. These results suggest that the holes are predominantly trapped in the bulk of the nanoparticle at low temperatures and at the surface at room temperature. So increasing the temperature increases the probability for the holes to be transferred to defects at the surface of the nanoparticles. It is interesting to note here that an exponential decay of the visible emission signal is also seen in *single crystals* at low temperatures (smaller than 20 K) with $\tau \simeq 0.44 \mu\text{s}$,⁶ a value similar to the one seen for $R = 3$ nm nanoparticles at $T = 4$ K quoted above. The transition from low to room temperatures seen by van Dijken et al.¹⁰ is at $T \sim 100 - 125$ K or $k_B T \simeq 0.01$ eV. The binding energy of the hole can depend on whether it is trapped at the center or at the surface of the nanoparticle and a difference in binding energies on the order of 0.01 eV is enough to thermally populate/depopulate one or the other site at that transition temperature. In general, there would be a spatial distribution of traps within the nanoparticle leading to a multiexponential decay of the luminescent signal with exponents than depend on the site where the trap is localized. The calculations of Figure 5, however, differ from the experimental results in that the theoretical position of the maximum moves to lower energies by 0.05 eV at most while differences of ca. 0.1 eV are found in the experiment, see Figure 5B of van Dijken et al.¹⁰ It could be that the interaction of the localized hole with the vibronic modes, which is certainly temperature dependent, also affects its energetic position, an important effect not considered in the present work.

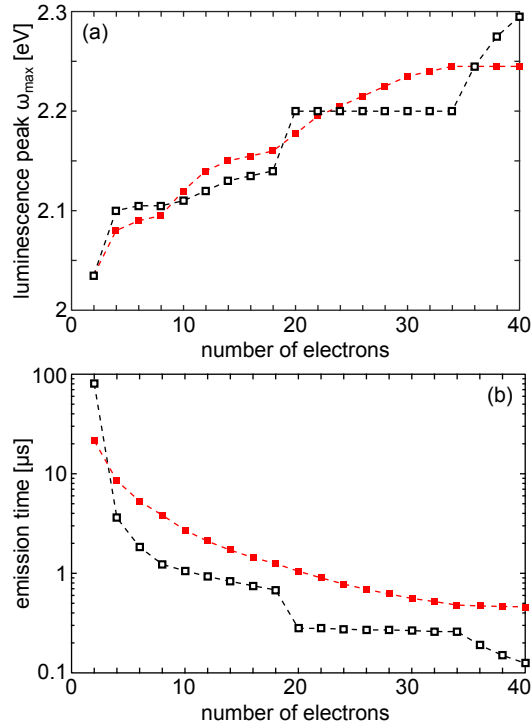


Figure 6: (a) Position in energy of the maximum of the visible luminescence spectra and (b) radiative time as a function of the number of conduction band electrons for ZnO nanospheres of $R = 4.5$ nm in toluene for $a = 0.2R$ (black open squares) and $a = 0.8R$ (red full squares). While the maximum energy blue-shifts with increasing number of electrons by $\approx 10\%$ the radiative time strongly decreases and only tends to saturate at large values of N_e .

Very recently it has been verified experimentally that air-free QDs of different sizes that are photodoped to the same doping level, all reach the same average value of their electronic density independent of size, at $n_e \gtrsim 0.2 \times 10^{20} \text{ cm}^{-3}$.³² The better agreement between theory and experiment, which we find under the assumption that the density of conduction band electrons is independent of size, implies that this is also the case in the presence of air. This is in accordance with other experimental observations such as, for example, Cohn et al.¹⁵ who “conclude a surprisingly high probability of exciting unintentionally charged ZnO nanocrystals even under aerobic conditions and even without deliberate addition of hole scavengers” and other works^{12,13} which find that it is more easy to charge with electrons the biggest crystals than the smaller ones. Hence it is important to analyze the dependence of the visible emission characteristics with electron density and we do it by considering a system of ZnO nanoparticles in toluene ($\epsilon_m = 2.25$), where it is known that they can be charged up to a maximum electron density of $n_e \approx 1 \times 10^{20} \text{ cm}^{-3}$.¹⁸ As in the work of Cohn et al.¹⁵ we consider spheres of $R = 4.5 \text{ nm}$ and present our results for ω_{max} and τ_{ph} as a function of N_e in Figure 6a,b, respectively. In this case, the maximum density is obtained for $N_e = 36$ electrons. As the number of electrons increases, the maximum of the spectra in Figure 6a blue shifts by 0.20–0.25 eV, that is $\approx 10\%$ at most, in accordance with other findings.^{12,14,17} The jumps in the value and/or slope of ω_{max} seen at $N_e = 4, 10, 20$ and 36 occur when a new shell starts to be filled. In contrast to ω_{max} , the radiative time shows a pronounced decrease for small N_e and tends to saturate for larger values. Experiments by Cohn et al.¹⁵ for uncharged crystals report a multiexponential decay that is fitted reasonably well by two time constants, a fast one of $\tau_1 \approx 0.2 \mu\text{s}$ and a slow one of $\tau_2 \approx 1.8 \mu\text{s}$, with the slow component constituting $\approx 90\%$ of the amplitude. Assigning this component to the radiative decay of holes localized near the surface, that value of τ_2 is obtained in our calculation for $N_e \approx 14$ electrons, or $n_e \approx 0.4 \times 10^{20} \text{ cm}^{-3}$, a value of the electron density similar to the one found above for reproducing experiments of aerated ZnO QDs in ethanol. However, the calculated radiative lifetime decreases continuously when increasing N_e above this value which seems

to be in contradiction with the observation of Cohn et al.¹⁵ who report that the slow component is weakly affected by the addition of extra electrons, but the effect is not quantified. Nevertheless, it is known that the accumulation of electrons in the conduction band strongly perturbs the dynamics of the trapped holes^{8-15,17} and, consequently, their decay time will be equally perturbed. Therefore, although our simple theoretical model is able to reproduce many experimental trends, we conclude that improvement of the theory as well as a better experimental characterization of the charge and distribution of defects in the nanocrystals is essential to fully understand and control the luminescent properties of ZnO QDs.

Conclusions

In this work we have developed a theory for the photoluminescence of ZnO QDs using Fermi's golden rule together with a simple model for the electronic states. We assumed the green luminescence to be generated in the radiative recombination of a delocalized conduction band electron with a hole trapped within the particle and analyzed the dependence of the spectral characteristics on the particle size and spatial localization of the hole. The behavior of this band with particle size can be understood in terms of quantum size effects of the electronic states and their overlap with the localized hole. Focusing the comparison of our results with the detailed experiments performed for ZnO nanoparticles in ethanol under aerobic conditions,^{10,11} we conclude that the experimental trends found at room temperature can be accurately reproduced by assuming that the hole is located at the surface of the QD. Based on our results of the dependence of emission intensity on the location of the hole, we suggest that the anomalous dependence of the decay time with temperature found by van Dijken et al.¹⁰ for $R = 3$ nm can be the effect of an increasing probability for the holes to be trapped at the surface with increasing temperature. Furthermore, the calculated values of the radiative lifetimes are comparable to the experimental values of the decay time of the visible emission signal. We also studied the visible emission band as a function of the

number of conduction band electrons in the nanoparticle finding a pronounced dependence of the radiative lifetime that does not seem to conform to experiment. We thus conclude that further improvement of the theoretical model, as well further experimental effort providing a better characterization of the distribution of traps and the charge of the nanoparticles, is essential to fully understand and control their emission properties.

Acknowledgement

RCM acknowledges financial support from the Spanish Ministry of Economy and Competitiveness through the María de Maeztu Programme for Units of Excellence in R&D (MDM-2014-0377) and the project MAT2014-53432-C5-5-R. TJA thanks the Polish Ministry of Science and Higher Education for support via the Iuventus Plus project IP2014 000473. TJA and SPA acknowledge financial support from the Swedish Foundation for Strategic Research via the Functional Electromagnetic Metamaterials for Optical Sensing project SSF RMA 11.

Supporting Information Available

The following files are available free of charge. In the Supporting Information we present full derivations of the calculations of overlap integrals and matrix elements.

References

- (1) Shrader, R. E.; Leverenz, H. W. Cathodoluminescence Emission Spectra of Zinc-Oxide Phosphors. *J. Opt. Soc. Am.* **1947**, *37*, 939–940.
- (2) Heiland, G.; Mollwo, E.; Stöckmann, F. In *Electronic Processes in Zinc Oxide*; Seitz, F., Turnbull, D., Eds.; Solid State Physics Supplement C; Academic Press, 1959; Vol. 8; pp 191–323.

- (3) Look, D. Recent advances in ZnO materials and devices. *Materials Science and Engineering: B* **2001**, *80*, 383–387.
- (4) Anpo, M.; Kubokawa, Y. Photoluminescence of zinc oxide powder as a probe of electron-hole surface processes. *The Journal of Physical Chemistry* **1984**, *88*, 5556–5560.
- (5) Vanheusden, K.; Warren, W. L.; Seager, C. H.; Tallant, D. R.; Voigt, J. A.; Gnade, B. E. Mechanisms behind green photoluminescence in ZnO phosphor powders. *Journal of Applied Physics* **1996**, *79*, 7983–7990.
- (6) Dingle, R. Luminescent Transitions Associated With Divalent Copper Impurities and the Green Emission from Semiconducting Zinc Oxide. *Phys. Rev. Lett.* **1969**, *23*, 579–581.
- (7) Kröger, F. A.; Vink, H. J. The Origin of the Fluorescence in Self-Activated ZnS, CdS, and ZnO. *The Journal of Chemical Physics* **1954**, *22*, 250–252.
- (8) Koch, U.; Fojtik, A.; Weller, H.; Henglein, A. Photochemistry of semiconductor colloids. Preparation of extremely small ZnO particles, fluorescence phenomena and size quantization effects. *Chemical Physics Letters* **1985**, *122*, 507–510.
- (9) Bahnemann, D. W.; Kormann, C.; Hoffmann, M. R. Preparation and characterization of quantum size zinc oxide: a detailed spectroscopic study. *The Journal of Physical Chemistry* **1987**, *91*, 3789–3798.
- (10) van Dijken, A.; Meulenkamp, E. A.; Vanmaekelbergh, D.; Meijerink, A. The Kinetics of the Radiative and Nonradiative Processes in Nanocrystalline ZnO Particles upon Photoexcitation. *The Journal of Physical Chemistry B* **2000**, *104*, 1715–1723.
- (11) van Dijken, A.; Meulenkamp, E. A.; Vanmaekelbergh, D.; Meijerink, A. Identification of the transition responsible for the visible emission in ZnO using quantum size effects. *Journal of Luminescence* **2000**, *90*, 123–128.

- (12) van Dijken, A.; Meulenkaamp, E. A.; Vanmaekelbergh, D.; Meijerink, A. Influence of Adsorbed Oxygen on the Emission Properties of Nanocrystalline ZnO Particles. *The Journal of Physical Chemistry B* **2000**, *104*, 4355–4360.
- (13) Stroyuk, O. L.; Dzhagan, V. M.; Shvalagin, V. V.; Kuchmiy, S. Y. Size-Dependent Optical Properties of Colloidal ZnO Nanoparticles Charged by Photoexcitation. *The Journal of Physical Chemistry C* **2010**, *114*, 220–225.
- (14) Yamamoto, S. Photoenhanced Band-Edge Luminescence in ZnO Nanocrystals Dispersed in Ethanol. *The Journal of Physical Chemistry C* **2011**, *115*, 21635–21640.
- (15) Cohn, A. W.; Janßen, N.; Mayer, J. M.; Gamelin, D. R. Photocharging ZnO Nanocrystals: Picosecond Hole Capture, Electron Accumulation, and Auger Recombination. *The Journal of Physical Chemistry C* **2012**, *116*, 20633–20642.
- (16) Shim, M.; Guyot-Sionnest, P. Organic-Capped ZnO Nanocrystals: Synthesis and n-Type Character. *Journal of the American Chemical Society* **2001**, *123*, 11651–11654, PMID: 11716721.
- (17) Fauchaux, J. A.; Jain, P. K. Plasmons in Photocharged ZnO Nanocrystals Revealing the Nature of Charge Dynamics. *The Journal of Physical Chemistry Letters* **2013**, *4*, 3024–3030.
- (18) Schimpf, A. M.; Thakkar, N.; Gunthardt, C. E.; Masiello, D. J.; Gamelin, D. R. Charge-Tunable Quantum Plasmons in Colloidal Semiconductor Nanocrystals. *ACS Nano* **2014**, *8*, 1065–1072.
- (19) Kilina, S. V.; Tamukong, P. K.; Kilin, D. S. Surface Chemistry of Semiconducting Quantum Dots: Theoretical Perspectives. *Accounts of Chemical Research* **2016**, *49*, 2127–2135, PMID: 27669357.

- (20) Giansante, C.; Infante, I. Surface Traps in Colloidal Quantum Dots: A Combined Experimental and Theoretical Perspective. *The Journal of Physical Chemistry Letters* **2017**, *8*, 5209–5215, PMID: 28972763.
- (21) Camarda, P.; Messina, F.; Vaccaro, L.; Agnello, S.; Buscarion, G.; Schneider, R.; Popescu, R.; Gerthsen, D.; Lorenzi, R.; Gelardi, F. M.; Cannas, M. Luminescence Mechanisms of Defective ZnO Nanoparticles. *Phys. Chem. Chem. Phys.* **2016**, *18*, 16237–16244.
- (22) Apell, P.; Ljungbert, A. A General Non-Local Theory for the Electromagnetic Response of a Small Metal Particle. *Physica Scripta* **1982**, *26*, 113–118.
- (23) Monreal, R. C.; Antosiewicz, T. J.; Apell, S. P. Diffuse Surface Scattering in the Plasmonic Resonances of Ultralow Electron Density Nanospheres. *The Journal of Physical Chemistry Letters* **2015**, *6*, 1847–1853.
- (24) Monreal, R. C.; Antosiewicz, T. J.; Apell, S. P. Diffuse Surface Scattering and Quantum Size Effects in the Surface Plasmon Resonances of Low-Carrier-Density Nanocrystals. *J. Phys. Chem. C* **2016**, *120*, 5074–5082.
- (25) Monreal, R. C.; Antosiewicz, T. J.; Apell, S. P. Competition between surface screening and size quantization for surface plasmons in nanoparticles. *New J. Phys* **2013**, *15*, 083044.
- (26) Gorkov, L. P.; Eliashberg, G. M. Minute metallic particles in an electromagnetic field. *Sov. Phys. JETP* **1965**, *21*, 940–947.
- (27) Janotti, A.; Van de Walle, C. G. Native point defects in ZnO. *Phys. Rev. B* **2007**, *76*, 165202.
- (28) Norberg, N. S.; Gamelin, D. R. Influence of Surface Modification on the Luminescence

- of Colloidal ZnO Nanocrystals. *The Journal of Physical Chemistry B* **2005**, *109*, 20810–20816, PMID: 16853697.
- (29) Löwdin, P.-O. On the Non-Orthogonality Problem Connected with the Use of Atomic Wave Functions in the Theory of Molecules and Crystals. *The Journal of Chemical Physics* **1950**, *18*, 365–375.
- (30) Monreal, R. C.; Apell, S. P.; Antosiewicz, T. J. Infrared Absorption and Hot Electron Production in Low-Electron-Density Nanospheres: A Look at Real Systems. *The Journal of Physical Chemistry Letters* **2017**, *8*, 524–530, PMID: 28067530.
- (31) Schlesinger, R.; Xu, Y.; Hofmann, O. T.; Winkler, S.; Frisch, J.; Niederhausen, J.; Vollmer, A.; Blumstengel, S.; Henneberger, F.; Rinke, P.; Scheffler, M.; Koch, N. Controlling the work function of ZnO and the energy-level alignment at the interface to organic semiconductors with a molecular electron acceptor. *Phys. Rev. B* **2013**, *87*, 155311.
- (32) Carroll, G. M.; Schimpf, A. M.; Tsui, E. Y.; Gamelin, D. R. Redox Potentials of Colloidal n-Type ZnO Nanocrystals: Effects of Confinement, Electron Density, and Fermi-Level Pinning by Aldehyde Hydrogenation. *Journal of the American Chemical Society* **2015**, *137*, 11163–11169, PMID: 26263400.